Journal of Polymers and the Environment (2020) 28:834–843
https://doi.org/10.1007/s10924-019-01647-0

ORIGINAL PAPER

Crystallization and Enzymatic Degradation of Maleic Acid-Grafted Poly(butylene adipate-co-terephthalate)/Organically Modified Layered Zinc Phenylphosphonate Nanocomposites

Hsiang-Ting Wang[1] · Erh-Chiang Chen[1] · Tzong-Ming Wu[1]

Published online: 1 January 2020

Abstract
Biodegradable nanocomposites were successfully synthesized using the maleic acid-grafted poly(butylene adipate-co-terephthalate) (g-PBAT) and organically modified layered zinc phenylphosphonate (m-PPZn), containing covalent linkages between g-PBAT and m-PPZn. Differential scanning calorimetry, wide-angle X-ray diffraction (WAXD), and transmission electron microscopy (TEM) were used to determine the crystallization behavior and morphology of g-PBAT/m-PPZn nanocomposites. The isothermal crystallization kinetics of g-PBAT/m-PPZn nanocomposites was determined using the Avrami equation. It was found that the half-time for the crystallization of the neat g-PBAT matrix is larger than that of g-PBAT/m-PPZn nanocomposites. This result suggests that the incorporation of m-PPZn can improve the crystallization rate of nanocomposites. The WAXD and TEM data illustrate that most of the m-PPZn layered materials are partially intercalated or exfoliated in the g-PBAT matrix. As the enzyme, lipase from *Pseudomonas* sp. was used for the enzymatic degradation tests. The degradation rates of the neatly fabricated g-PBAT copolymers using the heat pressing technique increase in the order of g-PBAT-80 > g-PBAT-50 > g-PBAT-20. The growing degradation rate of g-PBAT-80 is due to the growing amount of the adipate acid group and the increasing chain flexibility of the polymer backbone. Moreover, the increasing loading of m-PPZn enhances the weight loss of nanocomposites, suggesting that the existence of m-PPZn enhances the degradation of g-PBAT copolymers. The degradation rate of the freeze-drying samples containing a highly porous structure is greater than those prepared using the heat pressing technique.

Keywords Composites · Crystallization behavior · Enzymatic degradation

Introduction

Aliphatic–aromatic copolyesters have received considerable attention mainly because their polymer backbones contain favorable biodegradability of the aliphatic unit and outstanding physical properties of the aromatic unit [1, 2]. Among these aliphatic–aromatic copolyesters, poly(butylene adipate-co-terephthalate) (PBAT) is synthesized through transesterification and polycondensation using 1,4-butanediol, adipic acid, and terephthalic acid or dimethylene terephthalate [3–6]. PBAT contains excellent thermal and mechanical properties compared with those of poly(butylene succinate-co-adipate) (PBSA) [7, 8]. The addition of inorganic reinforcement to PBAT can improve its thermal and mechanical properties [9, 10].

Zhang et al. studied the effect of additional sugar beet pulp (SBP) on the morphology, rheology, and mechanical properties of PBAT/SBP blends [9]. Their experimental results showed that the incorporation of SBP into the PBAT matrix can enhance its tensile strength and modulus. Moustafa et al. demonstrated that the PBAT composites can be a potential candidate for food packaging applications [11]. However, only a previous study has discussed the enzymatic degradation behavior of PBAT copolymer [4]. To the best of our knowledge, no report has yet discussed the effect of the inorganic reinforcement on the crystallization behavior and enzymatic degradation of PBAT copolymer. Thus, the enzymatic degradation behavior of PBAT copolymer with the inorganic reinforcement is worth investigating.

✉ Tzong-Ming Wu
tmwu@dragon.nchu.edu.tw

[1] Department of Materials Science and Engineering, National Chung Hsing University, 250 Kuo Kuang Road, Taichung 402, Taiwan, ROC

Recently, the two-dimensional layered zinc phenylphosphonate (PPZn) has aroused considerable interest owing to the increasing crystallization rates of various polymers [12–14]. In our previous study, the biocompatible, nontoxic, and dual functional groups of 1, 12-dodecanediamine were utilized to prepare the organically-modified PPZn (o-PPZn) using the coprecipitation method [15]. A series of new biodegradable maleic acid-grafted poly(butylene adipate-co-terephthalate) (g-PBAT)/o-PPZn nanocomposites containing various weight ratios of o-PPZn were first reported and successfully synthesized with the covalent linkages between g-PBAT and o-PPZn. This experimental approach is crucial to prepare the porous g-PBAT nanocomposites without the phase separation of g-PBAT and o-PPZn.

In this report, 1, 6-diaminohexane, used as an organic modifier to enlarge the interlayer distance of PPZn (m-PPZn), was mixed with g-PBAT using the same methodology presented previously [15]. The enzymatic degradation and crystallization behaviors of various weight ratios of g-PBAT/m-PPZn nanocomposites were investigated. The effect of inorganic reinforcement on the morphology, crystallization behavior, and enzymatic degradability of biocompatible g-PBAT/m-PPZn nanocomposites was investigated. Finally, the porous structure of g-PBAT/m-PPZn nanocomposites was fabricated using the freeze-drying process. The effect of the porous structure on the enzymatic degradation behavior was also investigated.

Experimental

Materials

Adipate acid (AA), lipase from *Pseudomonas* sp., maleic acid (MA), phenylphosphonic acid, and zinc nitrate were obtained from Sigma-Aldrich Chemical Company., 1,4-butanediol (BD), 1, 6-diaminohexane, dimethylene terephthalate (DMT), 1-ethyl-3-(3-dimethylaminopropyl) carbodiimide (EDC), tetrabutyl titanate, and titanium(IV) butoxide were acquired from Alfa Aesar Chemical Company. Benzoyl peroxide was obtained from Fluka Chemical Company. 1, 4-Dioxane was purchased from Macron Fine Chemicals. All chemicals were used as received.

Fabrication of g-PBAT/m-PPZn Nanocomposites

Various molar ratios of g-PBAT-20, g-PBAT-50 and g-PBAT-80 were fabricated, grafted and reported previously [15]. In brief, desired amounts of AA, BD, DMT, and titanium(IV) butoxide as a catalyst were heated at 160 °C for 1 h, and then heated to 190 °C for 2 h to entirely distill water and methanol, and finally heated to 220 °C for 4 h in a vacuum of about 60 Pa. The PPZn and 1, 6-diaminohexane-modified PPZn (m-PPZn) were synthesized using the experimental method reported previously [16, 17]. For the fabrication of PPZn, the phenylphosphonic acid and zinc nitrate was individually dissolved in deionized water (DI-water) and mixed together followed by the addition of 0.1 M aqueous NaOH to reach pH 6. The prepared sample was filtered, washed, and dried at 60 °C for 3 days. Intercalation of 1, 6-diaminohexane was carried out by mixing about 0.2 g of PPZn with 20 ml 1, 6-diaminohexane at room temperature for 5 days. The resulting white solid was separated by filtration and dried at 60 °C for 10 h. Three weight ratios of g-PBAT/m-PPZn nanocomposites were synthesized with covalent bonds between the polymer and inorganic materials using the same methodology investigated in previous report [15]. To fabricate the specimens for further analyses, the 0.5 g g-PBAT/m-PPZn nanocomposites were heat pressed at the temperature about 20 °C above corresponding melting temperatures. For the preparation of porous structure used in the enzymatic degradation test, the 0.5 g g-PBAT/m-PPZn nanocomposites were dissolved in 100 ml 1, 4-dioxane. Since the g-PBAT-20 can't fully dissolve in 1, 4-dioxane, the following preparation was carried out for the g-PBAT-50, g-PBAT-80 and their related nanocomposites. The mixed solution poured into a polypropylene test tube, which was gradually moved at a rate of 6.8 mm/min into a liquid nitrogen bath to solidify the mixed solution. After entirely freezing the solution, the solidified specimen was freeze-drying for 48 h.

Methods

The isothermal crystallization behavior was obtained by a PerkinElmer Pyris Diamond differential scanning calorimetry (DSC, Waltham, MA, USA). All experiments measured under a nitrogen atmosphere were heated at a heating rate of 10 °C/min to a selected temperature, which was about 20 °C above corresponding melting temperature (T_m^0). The samples held for 5 min to eliminate the thermal history were then immediately cooled to proposed isothermal crystallization temperatures (T_{cs}) and held to completely finish the isothermal crystallization. The enthalpy of fusion (ΔH_f) recorded by heating scan was used to calculate the degree of crystallinity (Xc) according to a previous report [15]. Avrami equation was used to determine the isothermal crystallization kinetics and could be illustrated as follows: [18, 19]

$$1 - X_t = \exp(-kt^n), \tag{1}$$

where X_t is relative degree of crystallinity at crystallization time t, k is the crystallization rate constant, and n is the Avrami exponent. Equation (1) can be transferred into its natural logarithm form as follows:

$$\ln\left[-\ln\left(1-X_t\right)\right] = n\ln t + \ln k. \quad (2)$$

The half-time of crystallization, $t_{1/2}$, is the time at which the X_t is equal to 50%, which is identified using Eq. (3).

$$t_{1/2} = \left(\frac{\ln 2}{k}\right)^{1/n}. \quad (3)$$

Wide-angle X-ray diffraction (WAXD) experiments were operated using an X-ray diffractometer (Bruker D8, Karlsruhe, Germany) with Ni-filtered Cu Kα radiation source. The diffraction patterns were obtained in the range of 2θ = 1.5°–30° at a scanning rate of 1°/min. The measurement of transmission electron microscopy (TEM) was carried out using JEOL JEM-2010 (Tokyo, Japan). Samples of TEM measurements were prepared by a Reichert Ultracut ultramicrotome.

For the enzymatic degradation, the heat pressing and freeze-drying samples were cut into 10 mm × 10 mm. The average thickness of the samples is about 0.1 mm. The weights of the heat pressing and freeze-drying samples were about 20 and 5 mg, respectively. The test samples were performed using 24-well plates with 1 ml/mg lipase from *Pseudomonas* sp. The 1 ml/mg lipase from *Pseudomonas* sp. was distributed evenly to a 24-well plate in which the g-PBAT/m-PPZn nanocomposites were placed in each well. The 24-cell plate was then placed in a shaking incubator at 37 °C, 100 rpm, and 50% relative humidity (RH). The PBAT-80 and its related nanocomposites samples were removed at 12, 24, 36, 48, and 60 h, washed with DI-water and vacuum dried. The samples of PBAT-50, PBAT-20, and their related nanocomposites were removed at 3, 6, 9, 12, and 15 days, washed with DI-water and vacuum dried. The amount of enzymatic degradation was evaluated using the equation: $W_{weight\ loss}\ (\%) = 100[(W_0 - W_t)/W_0]$, where W_0 is the initial weight of a sample and W_t is the weight of a test sample after a choice of degradation times. The average values of experimental data shown here are obtained from at least three measurements. After the enzymatic degradation, the gel permeation chromatography (GPC; Waters 717 PlusAutosampler, Milford, MA, USA) was used to determine the.number-average molecular weight (M_n), weight-average molecular weight (M_w), and polydispersity PDI = M_w/M_n of the synthesizing polymers and composite materials. Polystyrene standards containing narrow molecular-weight distributions were employed as calibration. Field-emission scanning electron microscopy (FESEM) operated on JEOL JSM-6700F (Tokyo, Japan) was used to observe the morphologies after the enzymatic degradation. All specimens were coated with gold to avoid charging.

Results and Discussion

Structure and Morphology of g-PBAT/m-PPZn Nanocomposites

The X-ray diffraction curves of g-PBAT/m-PPZn nanocomposites displayed in Fig. 1 were used to investigate the structure of nanocomposites. For comparison, the X-ray diffraction profile of m-PPZn is also shown in this figure. Two diffraction peaks at 2θ = 3.98° and 7.86° were observed for 5 wt% g-PBAT-80/m-PPZn nanocomposites, which contributed to the stacking layers of m-PPZn [16, 17, 20]. No diffraction peaks were observed in the experimental data of the lower incorporation of m-PPZn. These results suggest a combination of intercalated and exfoliated microstructure for g-PBAT-80/m-PPZn nanocomposites, which is also consistent with previous report [21]. Similar structural information was also obtained for g-PBAT-50/m-PPZn and g-PBAT-20/m-PPZn nanocomposites.

Furthermore, the morphology of g-PBAT/m-PPZn nanocomposites was examined using the transmission electron microscopy (TEM) technique. Figure 2 demonstrates the TEM micrograph of 5 wt% g-PBAT-80/m-PPZn nanocomposites. The TEM micrograph shows that the stacking layers of m-PPZn are partially intercalated or exfoliated within the g-PBAT-80 copolyesters. Similar TEM images were also recorded for 5 wt% g-PBAT-50/m-PPZn and g-PBAT-20/m-PPZn nanocomposites. Hence, the partially intercalated or exfoliated morphologies of 5 wt% g-PBAT/m-PPZn

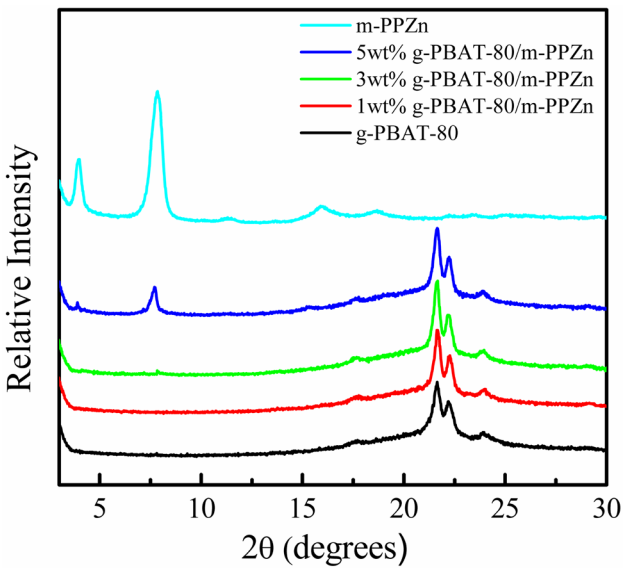

Fig. 1 WAXD patterns of g-PBAT-80, m-PPZn and various weight ratios of g-PBAT-80/m-PPZn nanocomposites

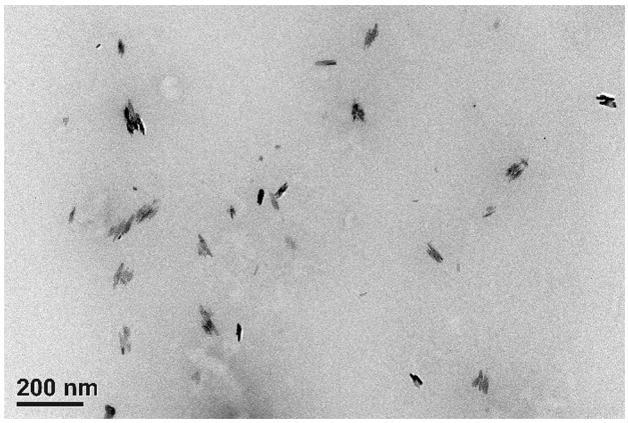

Fig. 2 TEM micrographs of 5 wt% g-PBAT-80/m-PPZn nanocomposites

nanocomposites observed using the TEM images are consistent with the wide-angle X-ray diffraction (WAXD) diffraction data.

Isothermal Crystallization Behavior of g-PBAT/m-PPZn Nanocomposites

The isothermal crystallization behaviors of g-PBAT copolymers with different m-PPZn concentrations were investigated to evaluate the influences of crystallization temperature (T_c) on the crystallization behavior of g-PBAT/m-PPZn nanocomposites. The Avrami plots of g-PBAT-80 and g-PBAT-80/m-PPZn nanocomposites at *various* T_{cs} are presented in Fig. 3. All the experimental curves are nearly parallel to each other, indicating that the crystallization mechanism is the same for g-PBAT-80 and g-PBAT-80/m-PPZn nanocomposites. Similar results were also obtained for g-PBAT-50/m-PPZn and g-PBAT-20/m-PPZn nanocomposites.

For comparison, Table 1 shows the *n*-values, *k*-values, and $t_{1/2}$ at various T_{cs} for all samples. The value of *n* characterizes the effectual criteria for the nucleation mechanism and the subsequent development of crystal growth. The experimental results indicate that the *n*-values of g-PBAT-80 are in the range of 2.72–3.06. In addition, the presence of a mixed growth and nucleation mechanism

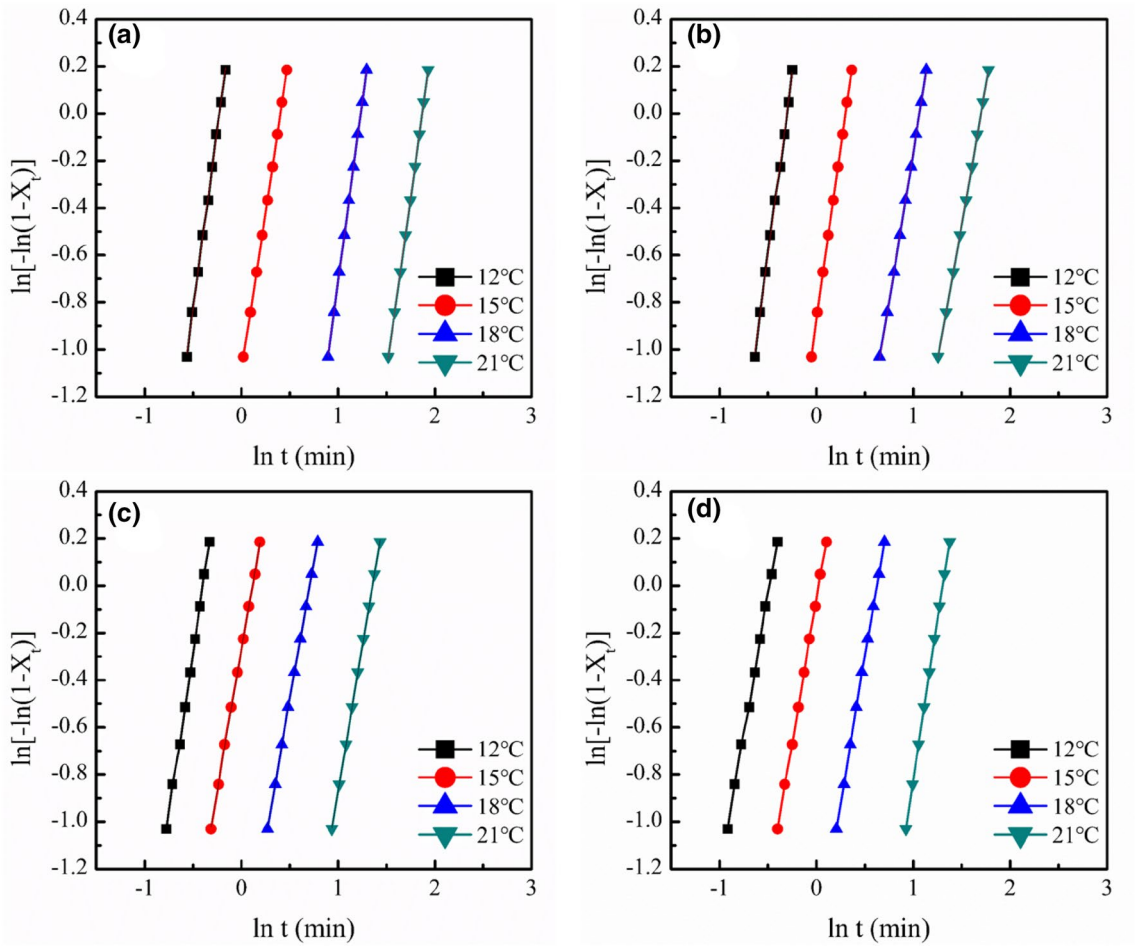

Fig. 3 Avrami plots of **a** g-PBAT-80, **b** 1 wt% g-PBAT-80/m-PPZn, **c** 3 wt% g-PBAT-80/m-PPZn, **d** 5 wt% g-PBAT-80/m-PPZn nanocomposites

Table 1 Kinetic parameters of neat g-PBAT and g-PBAT/m-PPZnnanocomposites isothermally melt crystallized at various T_c

Sample	T_c (°C)	n	K (min^{-n})	$t_{1/2}$ (min)
g-PBAT-80	12	3.03	1.99×10^{0}	0.71
	15	2.72	3.34×10^{-1}	1.31
	18	3.06	3.64×10^{-2}	3.04
	21	2.96	3.98×10^{-3}	5.73
1wt% g-PBAT-80/m-PPZn	12	3.07	2.55×10^{0}	0.65
	15	2.92	4.17×10^{-1}	1.19
	18	2.53	6.75×10^{-2}	2.51
	21	2.34	1.87×10^{-2}	4.68
3wt% g-PBAT-80/m-PPZn	12	2.73	2.97×10^{0}	0.59
	15	2.38	7.65×10^{-1}	0.96
	18	2.35	1.90×10^{-1}	1.73
	21	2.44	2.95×10^{-2}	3.34
5wt% g-PBAT-80/m-PPZn	12	2.35	3.12×10^{0}	0.53
	15	2.42	9.43×10^{-1}	0.88
	18	2.46	2.16×10^{-1}	1.61
	21	2.70	3.64×10^{-2}	3.22
g-PBAT-50	111	1.61	8.88×10^{-1}	0.86
	114	1.62	4.61×10^{-1}	1.29
	117	1.69	2.23×10^{-1}	1.96
	120	1.70	8.75×10^{-2}	3.39
1wt% g-PBAT-50/m-PPZn	111	1.75	9.81×10^{-1}	0.82
	114	1.57	5.10×10^{-1}	1.21
	117	1.52	3.03×10^{-1}	1.73
	120	1.41	1.33×10^{-1}	2.50
3wt% g-PBAT-50/m-PPZn	111	1.99	2.11×10^{0}	0.57
	114	1.75	7.18×10^{-1}	0.98
	117	1.73	3.05×10^{-1}	1.61
	120	1.80	1.93×10^{-1}	2.47
5wt% g-PBAT-50/m-PPZn	111	2.04	3.68×10^{0}	0.44
	114	1.96	1.45×10^{0}	0.69
	117	1.86	6.71×10^{-1}	1.02
	120	1.75	2.54×10^{-1}	1.77
g-PBAT-20	176	1.87	8.78×10^{-1}	0.88
	179	1.71	3.18×10^{-1}	1.58
	182	1.70	1.74×10^{-1}	2.25
	185	2.18	2.18×10^{-2}	4.90
1wt% g-PBAT-20/m-PPZn	176	1.88	2.81×10^{0}	0.48
	179	2.03	1.04×10^{0}	0.82
	182	2.29	1.98×10^{-1}	1.73
	185	2.35	2.88×10^{-2}	3.87
3wt% g-PBAT-20/m-PPZn	176	2.25	4.68×10^{0}	0.43
	179	2.08	1.17×10^{0}	0.78
	182	2.00	2.67×10^{-1}	1.61
	185	1.82	7.52×10^{-2}	3.39
5wt% g-PBAT-20/m-PPZn	176	2.25	6.36×10^{0}	0.37
	179	2.11	1.71×10^{0}	0.65
	182	2.06	3.07×10^{-1}	1.49
	185	1.88	7.97×10^{-2}	3.17

was used to illustrate the nonintegral n-values [22, 23]. Normally, the n-values close to 3.0 are attributed to a thermal nucleation mechanism, followed by the development of three-dimensional crystal growth. The n-values of g-PBAT-80/m-PPZn nanocomposites were found to range from 2.34 to 3.07, which are close to those of g-PBAT-80. These results suggest that the addition of m-PPZn to g-PBAT-80 copolymer does not change the crystallization mechanism of g-PBAT-80.

Furthermore, the crystallization kinetics of g-PBAT-80/m-PPZn nanocomposites can be discussed using the value of $t_{1/2}$, which increases in tandem with an increase in T_c. This result reveals that the isothermal crystallization rate decreases in tandem with an increase in T_c, which is attributed to lower supercooling at higher T_c. By adding 1 wt% m-PPZn to g-PBAT-80, $t_{1/2}$, as crystallized at $T_c = 21$ °C, significantly drops from 5.73 to 4.68 min. By adding more of m-PPZn to g-PBAT-80, $t_{1/2}$ continues dropping as the content of m-PPZn increases. These results indicate that the incorporation of m-PPZn into the polymer matrix, served as a heterogeneous nucleating agent, would significantly accelerate the crystallization of g-PBAT-80 in the nanocomposites.

The n-values, k-values, and $t_{1/2}$ at various T_{cs} for g-PBAT-50/m-PPZn and g-PBAT-20/m-PPZn nanocomposites are also shown in Table 1. The n-values of g-PBAT-50/m-PPZn and g-PBAT-20/m-PPZn nanocomposites are in the range of 1.41–2.04 and 1.70–2.35, respectively. The crystalline structure of g-PBAT-50 and g-PBAT-20 copolymers is in the crystalline form of PBT, which contains strict aromatic groups in the polymer backbone [15]. Therefore, the inclusion of stiff m-PPZn did not considerably influence the g-PBAT-50 and g-PBAT-20 polymer chains for diffusing and migrating them into the packing of PBT crystals.

The crystalline structure of g-PBAT-50/m-PPZn and g-PBAT-20/m-PPZn nanocomposites was also determined to be in the crystalline form of PBT. When crystallized at the same T_c, the $t_{1/2}$ of g-PBAT-50/m-PPZn and g-PBAT-20/m-PPZn nanocomposites is lower than that of pure g-PBAT-80. With the addition of more m-PPZn to g-PBAT, $t_{1/2}$ decreases in tandem with an increase in the content of m-PPZn. This result indicates that the presence of m-PPZn can accelerates the crystallization of PBT in nanocomposites, which is consistent with previous investigations [12–14]. The degree of crystallinity (Xc) estimated using the enthalpy of fusion (ΔH_f) of differential scanning calorimetry (DSC) heating curve is presented here. The values of Xc are 37.2, 36.9, 36.2, and 34.5 for g-PBAT-80, 1 wt% g-PBAT-80/m-PPZn, 3 wt% g-PBAT-80/m-PPZn, and 5 wt% g-PBAT-80/m-PPZn nanocomposites, respectively. A similar trend can also be observed for g-PBAT-50/m-PPZn and g-PBAT-20/m-PPZn nanocomposites.

Enzymatic Degradation of g-PBAT/m-PPZn Nanocomposites

For enzymatic degradation, two different fabricating techniques, namely heat pressing and freeze-drying, were utilized to generate change in surface morphology. The influences of m-PPZn on the enzymatic degradation of g-PBAT/m-PPZn nanocomposites were achieved by estimating the weight loss, calculating the change in molecular weight (M_w), and observing the change in surface morphology. Because m-PPZn cannot be degraded by means of lipase, the difference in weight loss, M_w, and surface morphology after enzymatic degradation experiments can be associated with g-PBAT copolymers.

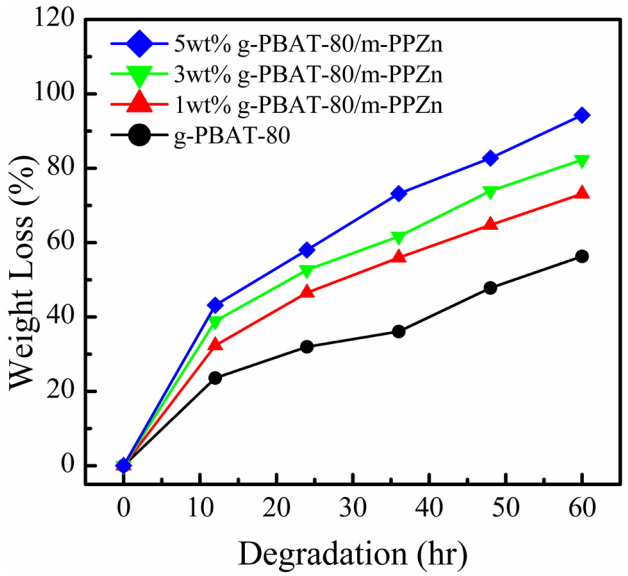

Fig. 4 Dependence of the weight loss on the degradation time for g-PBAT-80/m-PPZn nanocomposites prepared using the heat pressing proces

The weight losses of g-PBAT-80/m-PPZn nanocomposites using the heat pressing technique are shown in Fig. 4. The duration of the enzymatic degradation test depends on the time needed for almost the entire degradation of the specimens with higher degradation rate. After 60 h of enzymatic degradation, the weight loss was 94.26% for 5 wt% g-PBAT-80/m-PPZn nanocomposites. With the same degradation period for 5 wt% g-PBAT-80/m-PPZn nanocomposites, the weight losses for the neat g-PBAT-80 matrix, 1 wt% g-PBAT-80/m-PPZn, and 3 wt% g-PBAT-80/m-PPZn nanocomposites were observed to be around 56.3%, 73.2%, and 82.3%, respectively.

The weight losses of g-PBAT-50/m-PPZn and g-PBAT-20/m-PPZn nanocomposites showed similar tendencies, compared with those for g-PBAT-80/m-PPZn nanocomposites, although the degradation rates of both systems are much lower than those of g-PBAT-80. The degradation period of both systems should increase to 15 days, which is around six times the enzymatic degradation test for the g-PBAT-80 system. Table 2 displays the values of weight loss for all samples with various degradation periods. The degradation rate of g-PBAT-50 is faster than that of g-PBAT-20. The high amount of adipate acid unit and chain flexibility in the polymer backbone induces a fast degradation rate for g-PBAT-80 copolymer. Meanwhile, the increasing loading

Table 2 Weight loss of thermal-pressed g-PBAT/m-PPZn nanocomposites measured with various degradation times

Sample	Weight loss (%)				
	12 h[a]	24 h[a]	36 h[a]	48 h[a]	60 h[a]
	3 days[b]	6 days[b]	9 days[b]	12 days[b]	15 days[b]
g-PBAT-80[a]	23.58 ± 0.12	31.98 ± 0.13	36.09 ± 0.13	47.83 ± 0.18	56.32 ± 0.15
1 wt% PBAT-80/m-PPZn[a]	32.33 ± 0.14	46.49 ± 0.15	55.95 ± 0.20	64.76 ± 0.24	73.15 ± 0.18
3 wt% PBAT-80/m-PPZn[a]	38.89 ± 0.15	52.67 ± 0.19	61.68 ± 0.21	73.91 ± 0.26	82.30 ± 0.25
5 wt% PBAT-80/m-PPZn[a]	43.19 ± 0.16	58.02 ± 0.21	73.19 ± 0.25	82.7 ± 0.28	94.26 ± 0.31
g-PBAT-50[b]	7.02 ± 0.08	11.65 ± 0.09	14.49 ± 0.11	15.22 ± 0.12	19.78 ± 0.14
1 wt% PBAT-50/m-PPZn[b]	10.62 ± 0.08	15.83 ± 0.11	18.12 ± 0.12	22.11 ± 0.18	24.14 ± 0.19
3 wt% PBAT-50/m-PPZn[b]	14.29 ± 0.12	18.92 ± 0.15	21.78 ± 0.18	23.59 ± 0.21	26.88 ± 0.24
5 wt% PBAT-50/m-PPZn[b]	16.07 ± 0.14	21.31 ± 0.15	23.03 ± 0.19	26.34 ± 0.21	28.9 ± 0.22
g-PBAT-20[b]	0	0	1.43 ± 0.01	1.61 ± 0.01	2.08 ± 0.02
1 wt% PBAT-20/m-PPZn[b]	1.59 ± 0.01	2.45 ± 0.02	2.86 ± 0.02	3.58 ± 0.03	4.48 ± 0.03
3 wt% PBAT-20/m-PPZn[b]	1.96 ± 0.01	2.94 ± 0.02	3.89 ± 0.03	5.19 ± 0.04	6.33 ± 0.04
5 wt% PBAT-20/m-PPZn[b]	2.89 ± 0.01	3.63 ± 0.02	4.88 ± 0.03	7.32 ± 0.05	8.89 ± 0.07

[a]Degradation time for the neat g-PBAT-80 polymer matrix and g-PBAT-80/m-PPZn nanocomposites with various loadings of m-PPZn

[b]Degradation time for the neat g-PBAT-50, g-PBAT-20 polymer matrix and their related nanocomposites with various loadings of m-PPZn

of m-PPZn enhances the weight loss of nanocomposites, suggesting that the existence of m-PPZn enhances the degradation of g-PBAT copolymers. This result may contribute to a decrease in the degree of crystallinity in tandem with an increase in the incorporation of m-PPZn into the g-PBAT matrix.

The M_w and polydispersity index (PDI) of g-PBAT-80/m-PPZn nanocomposites during the enzymatic degradation are presented in Fig. 5. The experimental results indicate the highest M_w of 82 kDa and the lower PDI of 1.68 for g-PBAT-80 copolymer as compared with those of g-PBAT-80/m-PPZn nanocomposites. Neither the M_w nor the PDI of the tested samples altered substantially during the enzymatic degradation.

For g-PBAT-50/m-PPZn and g-PBAT-20/m-PPZN nanocomposites, analogous data were also collected. The M_w of g-PBAT-50/m-PPZn and g-PBAT-20/m-PPZN nanocomposites were approximately 75 and 31 kDa, respectively, with the PDI being in the range of 1.53–1.59. In accordance with the previous reports, the M_w and PDI of biodegradable polyesters, classified as exo-type hydrolysis activity, remained approximately constant as the number of biodegradable polyesters progressively decreased [24, 25]. Hence, our measurements suggest that the degradation mechanism of g-PBAT copolymer contributes to exo-type hydrolysis activity.

Figure 6 shows the change in morphology for the degraded g-PBAT-80/m-PPZn nanocomposites. Before degradation, the pure g-PBAT revealed a somewhat smooth surface compared with that of g-PBAT/m-PPZn nanocomposites. The surface roughness of g-PBAT-80 increased as the loading of m-PPZn increased. These results illustrate that the incorporation of m-PPZn can improve the degradation rate of g-PBAT-80 copolymer. After 60 h of enzymatic degradation, the porous structure of g-PBAT-80/m-PPZn nanocomposites was evident.

The porous structure of g-PBAT/m-PPZn nanocomposites was achieved using the freeze-drying method for the study of the effect of surface morphology on the enzymatic degradation rate of g-PBAT/m-PPZn nanocomposites. The synthesized g-PBAT/m-PPZn nanocomposites have the covalent linkages between g-PBAT and m-PPZn, which is a critical approach to prevent the phase separation of g-PBAT and m-PPZn during the freeze-drying process. Because g-PBAT-20 cannot fully dissolve in 1, 4-dioxane, the subsequent experiment was carried out for g-PBAT-50, g-PBAT-80, and their correlated nanocomposites.

The weight losses of g-PBAT-80/m-PPZn nanocomposites fabricated using the freeze-drying process are shown in Fig. 7. The enzymatic degradation period was kept the same to enable the comparison of the differences between the two different preparations. For g-PBAT-80/m-PPZn nanocomposites after 60 h of enzymatic degradation, the weight loss was 60.7% for neat g-PBAT-80; the weight losses for the 1 wt% g-PBAT-80/m-PPZn, 3 wt% g-PBAT-80/m-PPZn, and 5 wt% g-PBAT-80/m-PPZn nanocomposites with the same degradation time of g-PBAT-80 were around 85.0%, 95.5%, and 100%, respectively.

The values of weight losses for g-PBAT-50/m-PPZn nanocomposites fabricated using the freeze-drying process are listed in Table 3. The degradation rates of the porous g-PBAT-80/m-PPZn nanocomposites fabricated using the freeze-drying process are faster than those of g-PBAT-50/m-PPZn nanocomposites. This observation exhibits a similar tendency compared with the specimens prepared using the heat pressing process, although the degradation rates of the

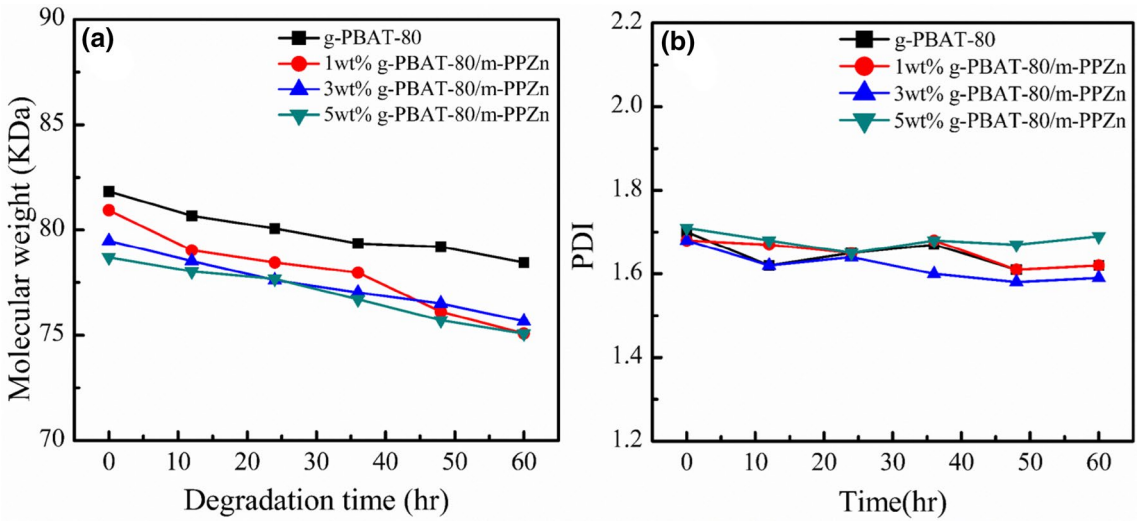

Fig. 5 **a** Molecular weight and **b** polydispersity index (PDI) of residual neat g-PBAT-80/m-PPZn nanocomposites after the enzymatic degradation

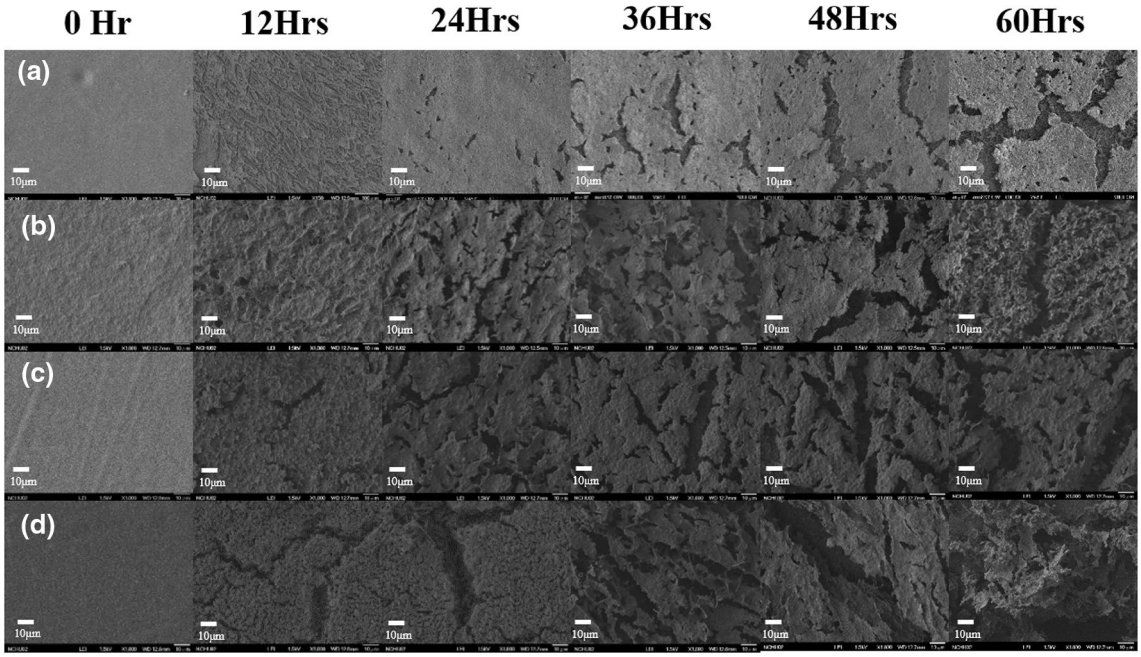

Fig. 6 FESEM images of the enzymatically degraded **a** PBAT-80, **b** g-PBAT-80, **c** 1 wt% g-PBAT-80/m-PPZn, **d** 3 wt% g-PBAT-80/m-PPZn nanocomposites, and **e** 5 wt% g-PBAT-80/m-PPZn nanocomposites prepared using the heat pressing process

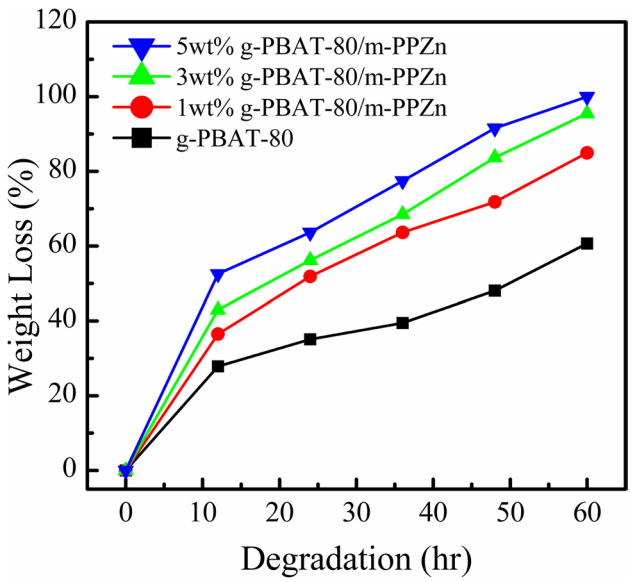

Fig. 7 Dependence of the weight loss on the degradation time for g-PBAT-80/m-PPZn nanocomposites prepared using the freeze-drying method

specimens fabricated using the freeze-drying process are much higher than those fabricated using the heat pressing process.

Figure 8 shows the FESEM micrographs of the degraded g-PBAT-80/m-PPZn nanocomposites. Before degradation, the pure g-PBAT-80 copolymer and its nanocomposites revealed various porous sizes. The pore sizes were slightly decreased in tandem with an increase in the incorporation of m-PPZn. The surface of g-PBAT-80/m-PPZn nanocomposite roughened after a 12 h degradation. This result illustrates that the incorporation of m-PPZn can enhance the degradation rate of g-PBAT-80 copolymer. The incorporation of 3 wt% and 5 wt% m-PPZn into g-PBAT-80 copolymers were further increased the degradation rate in tandem with an increase in the incorporation of m-PPZn.

Hence, it can be concluded that the degradation rate of g-PBAT copolymers significantly relies on the amount of adipate acid unit and the chain flexibility of the polymer backbone. The degradation rate of g-PBAT increases in tandem with an increase in the loading of m-PPZn, despite the chemical composition or crystalline structure of g-PBAT copolymers. At the same time, the degradation rates of g-PBAT copolymers with porous structures are higher than those of nonporous structures. Therefore, the enzymatic degradation behavior of g-PBAT can be considered a surface interaction process mainly because the size of the extracellular enzyme is too large to go through the interior of the polymer material. Thus, the majority of the interactions occur on the surface of the polymer [26].

The increasing contact of lipase with the g-PBAT polymer chain is probably due to the chemical nature of g-PBAT and the extra hydrophilic nature of m-PPZn, especially given that the m-PPZn content is comparatively high, yielding a porous morphology. Similar studies have investigated previously [26–29]. Thus, the amount of adipate acid unit and the

Table 3 Weight loss of freeze-drying g-PBAT/m-PPZn nanocomposites measured with various degradation times

Sample	Weight loss (%)				
	12 h[a]	24 h[a]	36 h[a]	48 h[a]	60 h[a]
	3 days[b]	6 days[b]	9 days[b]	12 days[b]	15 days[b]
g-PBAT-80[a]	27.84 ± 0.12	35.12 ± 0.15	39.47 ± 0.18	48.06 ± 0.21	60.66 ± 0.24
1 wt% PBAT-80/m-PPZn[a]	36.53 ± 0.14	51.85 ± 0.18	63.63 ± 0.21	71.82 ± 0.23	84.95 ± 0.32
3 wt% PBAT-80/m-PPZn[a]	42.98 ± 0.16	56.22 ± 0.20	68.49 ± 0.22	83.71 ± 0.25	95.46 ± 0.29
5 wt%PBAT-80/m-PPZn[a]	52.53 ± 0.16	63.67 ± 0.20	77.43 ± 0.25	91.57 ± 0.31	100
g-PBAT-50[b]	9.12 ± 0.02	12.04 ± 0.03	15.99 ± 0.06	17.41 ± 0.08	21.26 ± 0.11
1 wt% PBAT-50/m-PPZn[b]	13.16 ± 0.10	16.99 ± 0.12	21.72 ± 0.14	24.07 ± 0.16	27.42 ± 0.17
3 wt% PBAT-50/m-PPZn[b]	16.55 ± 0.11	19.63 ± 0.12	23.94 ± 0.14	26.63 ± 0.15	29.54 ± 0.18
5 wt%PBAT-50/m-PPZn[b]	18.71 ± 0.13	23.45 ± 0.16	25.64 ± 0.20	28.26 ± 0.21	31.85 ± 0.23

[a]Degradation time for the neat g-PBAT-80 polymer matrix and g-PBAT-80/m-PPZn nanocomposites with various loadings of m-PPZn

[b]Degradation time for the neat g-PBAT-50 polymer matrix and g-PBAT-50/m-PPZn nanocomposites with various loadings of m-PPZn

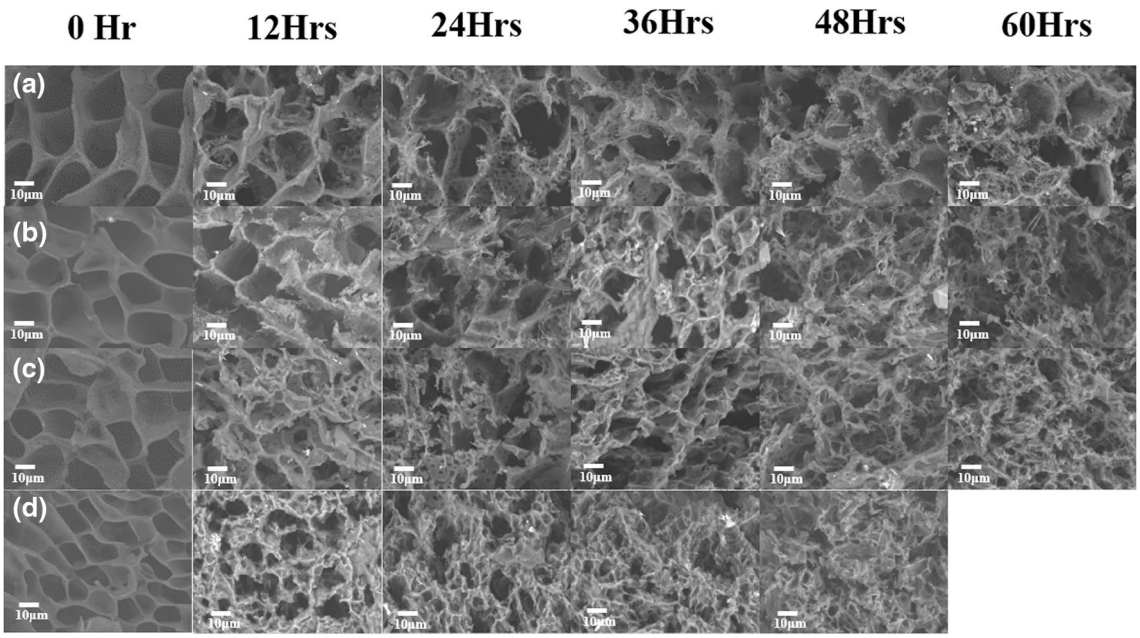

Fig. 8 FESEM images of the enzymatically degraded **a** g-PBAT-80, **b** 1 wt% g-PBAT-80/m-PPZn, **c** 3 wt% g-PBAT-80/m-PPZn nanocomposites, and **d** 5 wt% g-PBAT-80/m-PPZn nanocomposites prepared using the freeze-drying method

hydrophilic nature of materials containing a porous structure are the major issues affecting the degradation of g-PBAT/m-PPZn nanocomposites.

Conclusions

The biodegradable g-PBAT/m-PPZn nanocomposites containing covalent linkages between g-PBAT and m-PPZn were successfully prepared. The crystallization rate of g-PBAT/m-PPZn nanocomposites increases in tandem with an increase in the loading of m-PPZn. The enzymatic degradation rates of the pure g-PBAT copolymers prepared using the heat pressing method increased in the order of g-PBAT-80 > g-PBAT-50 > g-PBAT-20. The fastest degradation rate of g-PBAT-80 copolymer may be attributed to the higher quantity of adipate acid unit and the greater chain flexibility of the polymer backbone.

Furthermore, the weight loss increased in tandem with an increase in m-PPZn loading, suggesting that the inclusion of m-PPZn can enhance the degradation of g-PBAT copolymers. The degradation rate of the freeze-drying specimens

containing a highly porous structure is higher than that prepared using the heat pressing process. Therefore, the major issues affecting the degradation of g-PBAT/m-PPZn nanocomposites are attributed to the amount of adipate acid unit and the hydrophilic nature of materials containing a porous structure.

Acknowledgements This work is supported by the Ministry of Science and Technology (MOST) under Grant MOST 107-2221-E-005-020 and the Ministry of Education under the project of Innovation and Development Center of Sustainable Agriculture (IDCSA).

References

1. Tserki V, Matzinos P, Pavlidou E, Vachliotis D, Panayiotou C (2006) Biodegradable aliphatic polyesters. Part I. properties and biodegradation of poly(butylene succinate-co-butylene adipate). Polym Degrad Stab 91:367
2. Muller RJ, Kleeberg I, Deckwer WD (2001) Biodegradation of polyesters containing aromatic constituents. J Biotech 86:87
3. Gan Z, Kuwabara K, Yamamoto M, Abe H, Doi Y (2004) Solid-state structures and thermal properties of aliphatic–aromatic poly(butylene adipate-co-butylene terephthalate) copolyesters. Polym Degrad Stab 83:289
4. Zhao L, Gan Z (2006) Effect of copolymerized butylene terephthalate chains on polymorphism and enzymatic degradation of poly(butylene adipate). Polym Degrad Stab 91:2429
5. Shi XQ, Ito H, Kikutani T (2005) Characterization on mixed-crystal structure and properties of poly (butylene adipate-co-terephthalate) biodegradable fibers. Polymer 46:11442
6. Kijchavengkul T, Auras R, Rubino M, Alvarado E, Montero JRC, Rosales JM (2010) Atmospheric and soil degradation of aliphatic-aromatic polyester films. Polym Degrad Stab 95:99
7. Nikolic MS, Djonlagic J (2001) Synthesis and characterization of biodegradable poly(butylene succinate-co-butylene adipate)s. Polym Degrad Stab 74:263
8. Ojijo V, Cele H, Sinha Ray S (2011) Morphology and properties of polymer composites based on biodegradable polylactide/poly[(butylene succinate)-co-adipate] blend and nanoclay. Macromol Mater Eng 296:865
9. Liu B, Bhaladhare S, Zhan P, Jiang L, Zhang J, Liu L, Hotchkiss AT (2011) Morphology and properties of thermoplastic sugar beet pulp and poly(butylene adipate-co-terepthalate) blends. Ind Eng Chem Res 50:13859
10. Rodrigues BVM, Silva AS, Melo GFS, Vasconscellos LMR, Marciano FR, Lobo AO (2016) Influence of low contents of superhydrophilic MWCNT on the properties and cell viability of electrospun poly (butylene adipate-co-terephthalate) fibers. Mater Sci Eng C 59:782
11. Moustafa H, Guizani C, Dupont C, Martin V, Jeguirim M, Dufresne A (2017) Utilization of torrefied coffee grounds as reinforcing agent to produce high-quality biodegradable PBAT composites for food packaging applications. ACS Sustain Chem Eng 5:1906
12. Pan P, Liang Z, Cao A, Inoue Y (2009) Layered metal phosphonate reinforced poly(l-lactide) composites with a highly enhanced crystallization rate. ACS Appl Mat Interfaces 1:402
13. Xu T, Wang Y, He D, Xu Y, Li Q, Shen C (2014) Nucleation effect of layered metal phosphonate on crystallization of isotactic polypropylene. Polym Test 34:131
14. Yu F, Pan P, Nakamura N, Inoue Y (2011) Nucleation effect of layered metal phosphonate on crystallization of bacterial poly[(3-hydroxybutyrate)-co-(3-hydroxyhexanoate)]. Macromol Mater Eng 296:103
15. Wang HT, Wang JM, Wu TM (2019) Synthesis and characterization of biodegradable aliphatic-aromatic nanocomposites fabricated using maleic acid-grafted poly(butylene adipate-co-terephthalate) and organically modified layered zinc phenylphosphonate. Polym Int 68:1531
16. Poojary DM, Clearfield A (1995) Coordinative intercalation of alkylamines into layered zinc phenylphosphonate. Crystal structures from X-ray powder diffraction data. J Am Chem Soc 117:11278
17. Zhang Y, Scott KJ, Clearfield A (1995) Intercalation of alkylamines into dehydrated and hydrated phenylphosphonates. J Mater Chem 5:315
18. Avrami M (1940) Kinetics of phase change. II Transformation-time relations for random distribution of nuclei. J Chem Phys 8:212
19. Avrami M (1941) Granulation, phase change, and microstructure kinetics of phase change: III. J Chem Phys 9:177
20. Chen YA, Chen EC, Wu TM (2015) Organically-modified layered zinc phenylphosphonate reinforced stereocomplex-type poly(lactic acid) nanocomposites with the highly enhanced mechanical properties and degradability. J Mater Sci 50:7770
21. Chen YA, Chen EC, Wu TM (2016) Lamellae evolution of stereocomplex-type poly(lactic acid)/organically-modified layered zinc phenylphosphonate nanocomposites induced by isothermal crystallization. Materials 9:159
22. Alamo RG, Mandelkern L (1991) Crystallization kinetics of random ethylene copolymers. Macromolecules 24:6480
23. Chen YA, Wu TM (2014) Crystallization kinetics of poly(1,4-butylene adipate) with stereocomplexed poly(lactic acid) serving as a nucleation agent. Ind Eng Chem Res 53:16689
24. Hocking PJ, Marchessault RH, Timmins MR, Lenz RW, Fuller RC (1996) Enzymatic degradation of single crystals of bacterial and synthetic poly(β-hydroxybutyrate). Macromolecules 29:2472
25. Ciou CY, Li SY, Wu TM (2014) Morphology and degradation behavior of poly(3-hydroxybutyrate-co-3-hydroxyvalerate)/layered double hydroxides composites. Eur Polym J 59:136
26. Bikiaris DN (2013) Nanocomposites of aliphatic polyesters: an overview of the effect of different nanofillers on enzymatic hydrolysis and biodegradation of polyesters. Polym Degrad Stab 98:1908
27. Bikiaris DN, Nianias NP, Karagiannidou EG, Docoslis A (2012) Effect of different nanoparticles on the properties and enzymatic hydrolysis mechanism of aliphatic polyesters. Polym Degrad Stab 97:2077
28. Chen YA, Kuo DL, Chen EC, Wu TM (2017) Enhanced enzymatic degradation in nanocomposites of various organically-modified layered zinc phenylphosphonates and poly (butylene succinate-co-adipate). J Polym Res 24:212
29. Kuo DL, Wu TM (2019) Crystallization behavior and morphology of hexadecylamine-modified layered zinc phenylphosphonate and poly(butylene succinate-co-adipate) composites with controllable biodegradation rates. J Polym Environ 27:10